ISSN (Print) 1226-1750
ISSN (Online) 2233-6656
Journal of Magnetics 28(1), 1-5 (2023) https://doi.org/10.4283/JMAG.2023.28.1.001

Structure and Thermal-enhanced Magnetic Properties of Mn_4C Melt-spun Ribbons with Varied Stoichiometry

Ting-Ting Qi[1], Ping-Zhan Si[1]*, Fang Cheng[1], Zhi-Rui Wang[1], Hong-Liang Ge[1], Qiong Wu[1], Jihoon Park[2], and Chul-Jin Choi[2]

[1]*College of Materials Science and Chemistry, China Jiliang University, 310018, Hangzhou, China*
[2]*Powder & Ceramic Division, Korea Institute of Materials Science, 51508, Changwon, R. Korea*

(Received 1 October 2022, Received in final form 23 February 2023, Accepted 7 March 2023)

Cubic perovskite-type Mn_4C is difficult to prepare for its metastable characteristics. In this work, we have obtained high-purity Mn_4C successfully by using melt-spinning method. The effects of stoichiometry on the structure and magnetic properties of the samples were studied systematically. We found that $x = -0.1$ is the optimum composition for the formation of the cubic perovskite phase in $Mn_{4+x}C$ during rapid quenching. Most $Mn_{4+x}C$ melt-spun ribbons with x other than -0.1 are composed of $Mn_{23}C_6$, α-Mn, and Mn_4C, while the fraction of different phase in $Mn_{4+x}C$ ribbons varies with x. The Curie temperature of $Mn_{4+x}C$ ribbons increases slightly with decreasing x, which may affect the lattice parameters of cubic Mn_4C and thus the Mn-Mn exchange interactions. The magnetization of $Mn_{4+x}C$ ($x = -0.1$ and 0) increases with increasing temperature in high-temperature region while the onset temperature for such behavior is dependent on the fraction of Mn_4C in the samples.

Keywords : Mn_4C, magnetic properties, melt-spun ribbons

1. Introduction

The saturation magnetization of most magnetic materials decreases with increasing temperature due to thermal disruption on the magnetic ordering [1-3]. From technical point of view, it is highly desired to find magnetic materials that can resist thermal deterioration when operating at temperatures above room temperature. We recently found that Mn_4C exhibits positive temperature coefficient of magnetization over a wide temperature range [4]. The synthesis of cubic perovskite-type Mn_4C have been thought to be difficult for a long time due to its meta-stable characteristics. In 1951, Mitsutak Isobe reported on the equilibrium diagram of Mn-C alloy, in which a new phase with a composition seemed to be about Mn_4C was found to exist at room temperature in the range from 4.3 to 4.6 percent of carbon [5]. However, the new phase of Mn_4C reported by Isobe was later proved to be $Mn_{23}C_6$ [6, 7]. In 1954, Morgan reported on a weakly ferromagnetic Mn_4C alloy prepared by using water quenching with subsequent magnetic separation process [8]. Unfortunately, the Mn_4C reported by Morgan was soon suggested to be $Mn_4(C, O)$ [9, 10]. The introduction of O atoms, more or less, is inevitable when processing high-temperature Mn-C alloys in air and water, even though the processing time is short. In 1991, Karen *et al.* reported on the similar water quenching of Mn-C alloys with varied compositions which invariably gave a mixture of $Mn_{23}C_6$ and Mn instead of Mn_4C phase [11]. After that, no experimental work on Mn_4C could be found until 2018, in which we obtained high-purity Mn_4C powder by using arc melting followed by magnetic separation process [4]. However, the mechanisms for Mn_4C phase formation in our previous work are not clear and the production efficiency is relatively low [4]. In this work, we have prepared Mn_4C by using an alternative melt-spinning method. The rapid solidification process was conducted in vacuum/argon to prevent possible contamination of oxygen to our samples. The effects of Mn/C stoichiometry on the phase formation, structure, and magnetic properties of the Mn_4C products have been studied systematically.

*Corresponding author: Tel: +86-13221019908
e-mail: pzsi@mail.com

2. Experimental

The $Mn_{4+x}C$ master alloys with nominal composition of x = -0.3, -0.2, -0.1, 0, 0.1, 0.2, and 0.3 were prepared by induction melting of high-purity Mn and graphite in argon atmosphere and then cooling down naturally. A piece of the master alloy was placed in a quartz tube with an orifice of 0.6 mm in diameter at the bottom. After that, the alloy was induction-melted again and then ejected through the orifice with argon on a room temperature copper wheel that rotating at a surface velocity of 15 m/s. The melt-spun ribbons were cooled in argon and collected in air for subsequent characterizations.

The structure of the melt-spun ribbons was recorded at room temperature by using a Rigaku A/Max 2500 automatic X-ray diffractometer (XRD) operating at 40 kV with Cu-Kα radiation. The magnetic properties of the samples were measured by using a Quantum Design physical property measurement system (PPMS) in an applied magnetic field up to 3 T and at temperatures up to 940 K. The temperature dependence of magnetization of the samples was measured under an applied field of 1 T with an increasing temperature rate of 20 K/min.

3. Results and Discussion

As shown in Fig. 1(a), the XRD patterns of the $Mn_{4+x}C$ (x = 0, ±0.1, ±0.2, ±0.3) master alloys prepared by using induction melting could be indexed with $Mn_{23}C_6$ and α-Mn. However, the relative diffraction intensity of $Mn_{23}C_6$ and Mn varies with varying composition of x. No diffraction peaks for Mn_4C could be found in these samples, owing to the meta-stable characteristics of Mn_4C, which is absent in the equilibrium Mn-C binary phase diagrams [6]. The $Mn_{23}C_6$ is the stable phase in the compositional vicinity of Mn_4C. The fraction of $Mn_{23}C_6$ in the $Mn_{4+x}C$ master alloys increases with decreasing x in the composition range from x = 0.3 to x = -0.1. The presence of α-Mn in $Mn_{4+x}C$ with x = 0, 0.1, 0.2, and 0.3 is not strange for the precipitation of excess Mn during the formation of the $Mn_{23}C_6$ phase when cooling down. It is interesting that the fraction of $Mn_{23}C_6$ in the sample with x = -0.1 is also higher than that in the samples with x = -0.3 and -0.2, as shown in the relative intensity of the two phases in Fig. 1(a). Detailed studies showed that the diffraction peaks for $Mn_{23}C_6$ in $Mn_{4+x}C$ with x = -0.1, -0.2, and -0.3 shift to the lower angle in comparison with that of samples with x = 0, 0.1, 0.2, and 0.3, indicating lattice expansion of $Mn_{23}C_6$ obtained in samples with excess C, as shown in Fig. 1(a). We speculate that the excess small C atoms may present in the lattices of

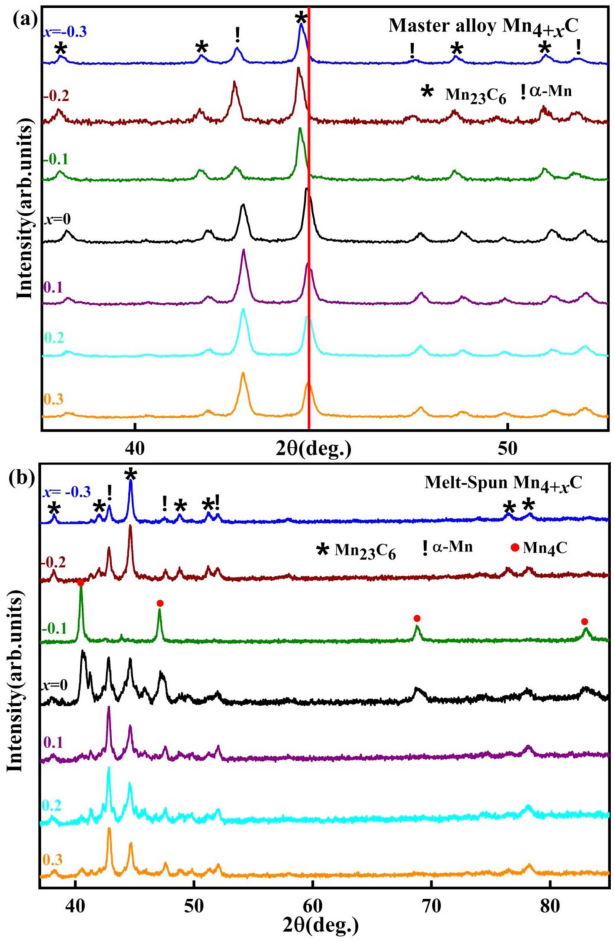

Fig. 1. (Color online) The X-ray diffraction patterns of the $Mn_{4+x}C$ master alloys (a) and the melt-spun ribbons (b) with varied x, respectively. The master alloys were mainly composed of $Mn_{23}C_6$ and α-Mn, while an additional phase of Mn_4C was found in the the melt-spun ribbons.

$Mn_{23}C_6$ and Mn as solid solution atoms for $Mn_{4+x}C$ with x < 0, and thus the lattices are expanded to some extent. However, for $Mn_{4+x}C$ with $x \geq 0$, the excess Mn atoms are difficult to present in the form of solid solution in $Mn_{23}C_6$ lattices for larger diameter of Mn atoms, and thus the lattice parameters of $Mn_{23}C_6$ varies little with x.

As shown in Fig. 1(b), the XRD patterns of the $Mn_{4+x}C$ melt-spun ribbons could be mainly indexed with Mn_4C, $Mn_{23}C_6$, and α-Mn for x = 0, 0.1, 0.2, and 0.3, Mn_4C for x = -0.1, $Mn_{23}C_6$ and Mn for x = -0.2 and -0.3, respectively. It seems excess Mn is detrimental for the formation of Mn_4C phase in the melt-spun ribbons, even though a small amount of Mn_4C was also formed in the ribbons with x = 0.1, 0.2, and 0.3. The fraction of Mn_4C phase in the melt-spun ribbons increased significantly in the x = 0 sample but a large fraction of $Mn_{23}C_6$ and Mn could also be found. High-purity Mn_4C phase was formed in the

$Mn_{4+x}C$ melt-spun ribbons with $x = -0.1$, indicating structural stabilizing effect of a small amount of excess carbon in the formation of metastable cubic perovskite-type Mn_4C. The structural stabilizing effect of C atoms has also been observed in MnAl(C) magnetic materials [12]. The diffraction peaks of Mn_4C in $x = -0.1$ is sharper than that in $x = 0$, indicating larger grain size of Mn_4C in $x = -0.1$ than that in $x = 0$. It is interesting that almost no Mn_4C phase was detected by XRD in samples with $x = -0.2$ and -0.3. However, we could not exclude the presence of Mn_4C phase in $x = -0.2$ and -0.3 for limited sensitivity of the XRD techniques. In fact, the subsequent magnetic measurements on $x = -0.2$ and -0.3 samples proved the presence of trace amount of ferrimagnetic Mn_4C phase in the samples. Most Mn-C binary alloyed phases, including $Mn_{23}C_6$, Mn_3C, Mn_5C_2, Mn_7C_3, and Mn(C) solid solutions, are paramagnetic at temperatures above room temperature. The XRD results proved that the stoichiometry of $Mn_{4+x}C$ has substantial effect on the formation of cubic Mn_4C phase.

Fig. 2 shows the temperature dependence of magnetization of the $Mn_{4+x}C$ melt-spun ribbons with a nominal composition of $x = -0.1$ and $x = 0$, respectively. The magnetization of $x = -0.1$ ribbons increases almost linearly with increasing temperature in the temperature range of 60 K to 608 K. The magnetization of $x = -0.1$ ribbons at 300 K is much higher than that of the sample at 5 K. The positive temperature coefficient of magnetization was further proved by the magnetic hysteresis loops of the $x = -0.1$ ribbons, as shown in Fig. 3. The enhanced magnetization with increasing temperature could be explained in terms of the Néel's P-type ferrimagnetism [13-15]. The Mn_4C has a simple cubic perovskite-type structure. The chemical formula of Mn_4C can be written as $(Mn_{II})_3Mn_IC$, where Mn_I is the corner atom, Mn_{II} is three face-centered atoms, and the carbon is at the body-centered position [4]. The two magnetic sublattices of Mn_I and Mn_{II} contributes to the total magnetization of Mn_4C. By using the Brillouin function to investigate the origin of the unusual linearly increasing magnetization, we found that the increasing magnetization is originated from strong mutual interdependence of more or less linearly decreasing magnetic moment of Mn_I atoms and stationary magnetic moment of Mn_{II} atoms [16]. The recent neutron-diffraction results of Mn_4C at 5 K showed that the refined ordered moments were -2.97(14) μ_B in the Mn_I site and 2.00(22) μ_B in the Mn_{II} site. When the temperature increased to 150 K, the refined Mn_I moment increased to -2.82 (11) μ_B, but the Mn_{II} moment remained 2.04(19) μ_B [17].

For $Mn_{4+x}C$ with $x = 0$, the onset temperature for positive temperature coefficient of magnetization is 170 K, which is much higher than the 60 K onset temperature observed in the $x = -0.1$ sample. We attribute the higher

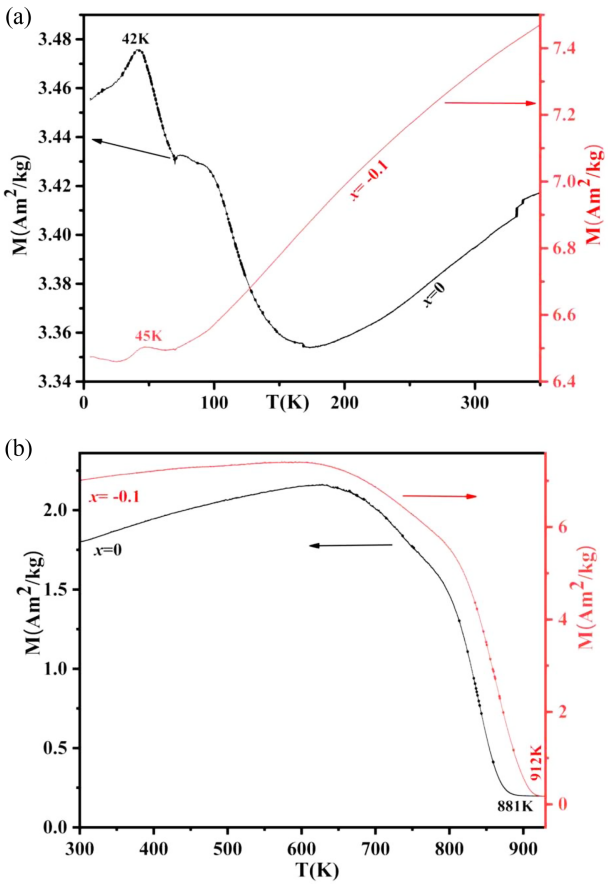

Fig. 2. (Color online) The temperature dependence of magnetization of the $Mn_{4+x}C$ melt-spun ribbons with $x = -0.1$ and $x = 0$, respectively.

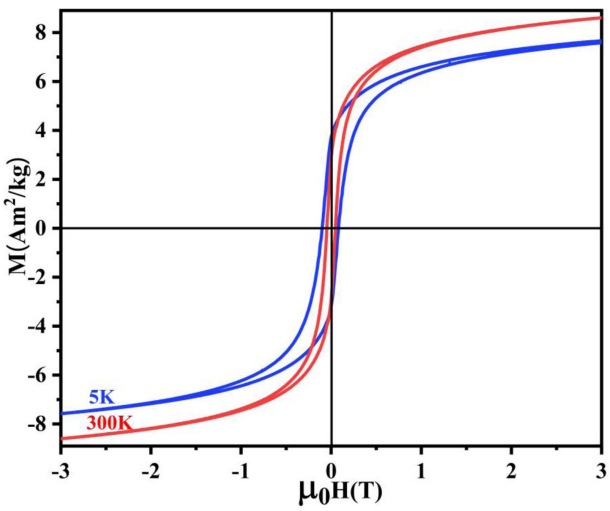

Fig. 3. (Color online) The magnetic hysteresis loops of $Mn_{4+x}C$ ($x = -0.1$) melt-spun ribbons at 5 K and 300 K, respectively.

onset temperature in $x = 0$ sample to the presence of higher fraction of $Mn_{23}C_6$ and Mn impurities, which exhibit decreasing magnetization with increasing temperature. The total magnetization of the sample is the sum of the phases with opposite M-T coefficients, positive for Mn_4C and negative for other phases.

The magnetization of $Mn_{4+x}C$ with $x = -0.1$ and 0 deceases slowly first from 610 K and 633 K, then sharply at 863 K and 839 K, and finally vanishes at 912 K and 881 K, respectively. The Curie temperature of the $x = -0.1$ sample is higher than that of the sample with $x = 0$. We attribute the varied T_C in different samples to the varied lattice parameters due to varied stoichiometry. It is known that the exchange coupling constants in manganese alloys is strongly affected by the Mn-Mn atomic distance [18, 19]. The grain size of the Mn_4C in the $Mn_{4+x}C$ ribbons with $x = -0.1$ and 0 is estimated by using Scherrer's formula to be 41.9 nm and 29.9 nm, respectively. Our XRD results showed that the Mn/C stoichiometry has substantial effect on the lattice parameters of both $Mn_{23}C_6$ and Mn_4C.

The magnetization of the $x = -0.1$ sample at temperatures below 30 K varies little with temperature and this behavior is quite similar to that in the Mn_4C samples prepared by arc melting and magnetic separation process [4]. A magnetic transition occurs at 43 K-45 K for unknown reason. The magnetization of the $x = -0.1$ sample at 1 T reached up to 7.48 Am^2/kg at 350 K while that of the $x = 0$ sample is merely 3.41 Am^2/kg, owing to the higher fraction of impurities in the $x = 0$ sample as seen in Fig. 1(b). The Mn_4C phase is ferrimagnetic and it contribute the majority of the magnetization of the

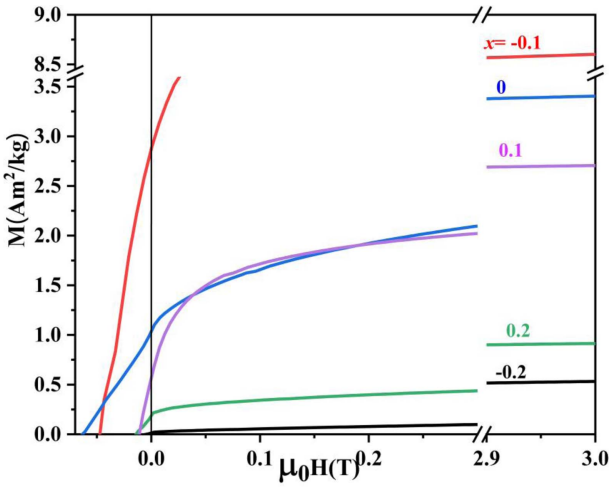

Fig. 4. (Color online) The M-H curves of the $Mn_{4+x}C$ melt-spun ribbons with varied x measured at 300 K.

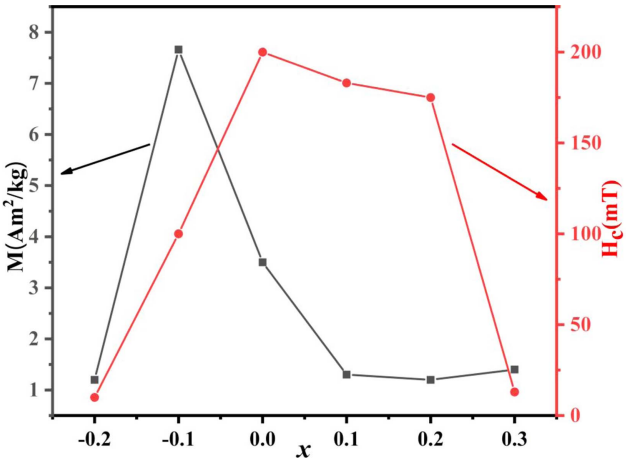

Fig. 5. (Color online) The compositional dependence of M_S and H_C in $Mn_{4+x}C$ melt-spun ribbons measured at 5 K.

samples for both $Mn_{23}C_6$ and Mn are antiferromagnetic or paramagnetic in the temperature region of 5 K-960 K. The variation of the lattice parameters and thus the exchange coupling constants may also contribute a variation of the magnetization of the samples.

Fig. 4 shows the magnetic hysteresis loops of the $Mn_{4+x}C$ melt-spun ribbons measured at 300 K and under an applied field up to 3 T. The M_S of the $x = -0.1$ sample is 8.61 Am^2/kg, which is much higher than that of the other samples, 3.4 Am^2/kg for $x = 0$, 2.7 Am^2/kg for $x = 0.1$, 0.93 Am^2/kg for $x = 0.2$, 0.54 Am^2/kg for $x = -0.2$, owing to the presence of varied fraction of ferrimagnetic Mn_4C in different samples. The remanent magnetization (2.84 Am^2/kg) of the $x = -0.1$ sample is also larger than that of the other samples. The coercivity of the $Mn_{4+x}C$ ribbons is in the range from 10 mT ($x = -0.2$) to 63 mT ($x = 0$). Both grain size and magnetic anisotropy field of the Mn_4C phase have effect on the coercivity of the samples. Fig. 1(b) shows that the diffraction peaks of Mn_4C phase in the $x = 0$ sample are broader than that in the $x = -0.1$ sample, indicating smaller grain size for the $x = 0$ sample. The presence of excess interstitial C atoms may also result in a slight change of the lattice parameters and thus the coercivity. The effect of composition on the M_S and H_C of the melt-spun ribbons measured at 5 K is plotted in Fig. 5. The M_S of the $x = -0.1$ sample at 5 K is 7.66 Am^2/kg. The coercivity of the $Mn_{4+x}C$ samples at 5 K is in the range from 10 mT ($x = -0.2$) to 200 mT ($x = 0$). The M-H loops of the $x = -0.2$ and -0.3 samples proved the presence of trace amount of ferrimagnetic Mn_4C phase in the samples, even though Mn_4C could not be indexed in the XRD patterns as mentioned above.

4. Conclusion

The $Mn_{4+x}C$ melt-spun ribbons with nominal compositions of x = -0.3, -0.2, -0.2, -0.1, 0, 0, 0.1, 0.2 and 0.3 were prepared by induction-melting with subsequent melt-quenching method. High-purity cubic perovskite-type Mn_4C was obtained in $Mn_{4+x}C$ with x = -0.1. This work provides an alternative novel method to prepare meta-stable Mn_4C phase. The Mn/C stoichiometry has substantial effect on the phase formation, structure, and magnetic properties of the Mn_4C-based products.

Acknowledgments

We appreciate the financial support from NSFC (No. 52271191), the fundamental research funds for the Provincial University of Zhejiang (Nos. 2019YW11 & 2020YW24), and the Creative Materials Discovery Program through the National Research Foundation of Korea (NRF) funded by the Ministry of Science, ICT and Future Planning (No. 2016M3D1A1027835). Note that this work was first submitted to Journal of Magnetism and Magnetic Mateirals in April, 2022.

References

[1] R. Peña-Garcia, Y. Guerra, D. Oliveira, A. Franco Jr, and E. Padrón-Hernández, Ceram. Int. **46**, 5871 (2020).
[2] L. Pierobon, R. E. Schäublin, A. Kovács, S. S. Gerstl, A. Firlus, U. V. Wyss, R. E. Dunin-Borkowski, M. Charilaou, and J. F. Löffler, J. Appl. Phys. **129**, 183903 (2021).
[3] S. Yuce, E. K. Doğan, B. Emre, N. Bruno, I. Karaman, and H. Yurtseven, J. Supercond. Nov. Magn. **30**, 3587 (2017).
[4] P. Z. Si, H. D. Qian, H. L. Ge, J. Park, and C. J. Choi, Appl. Phys. Lett. **112**, 192407 (2018).
[5] M. Isobe, Sci. Rep. Res. Inst. Tohuku Univ. **A3**, 468 (1951).
[6] D. Djurovic, B. Hallstedt, J. von Appen, and R. Dronskowski, Calphad **34**, 279 (2010).
[7] T. Y. Kosolapova, Carbides: properties, production, and applications, Plenum press, New York-London (1971) pp. 168.
[8] E. R. Morgan, JOM. **6**, 983 (1954).
[9] K. Kuo and L. E. Persson, J. Iron and Steel Inst. **178**, 39 (1954).
[10] R. Benz, J. F. Elliott, and J. Chipman, Metall. Mater. Trans. B **4**, 1449 (1973).
[11] P. Karen, H. Fjellvåg, A. Kjekshus, A. Andresen, and I. Trabjerg, Acta Chem. Scand. **45**, 549 (1991).
[12] P. Z. Si, H. D. Qian, C. J. Choi, J. Park, S. Han, H. L. Ge, and K. P. Shinde, Materials **10**, 1016 (2017).
[13] L. Néel, Ann. Phys.-Paris. **12**, 137 (1948).
[14] J. S. Smart, Am. J. Phys. **23**, 356 (1955).
[15] P. Z. Si, J. T. Lim, J. Park, and C. J. Choi, Powder Diffr. **34**, 196 (2019).
[16] J. Park, H. D. Qian, P. Z. Si, and C. J. Choi, J. Magn. Magn. Mater. **527**, 167765 (2021).
[17] F. G. Wang, S. H. Fan, Z. C. Lin, B. C. Wu, W. Y. Yang, C. S. Wang, Q. Xu, S. Q. Liu, J. B. Yang, H. L. Du, and J. Z. Han, J. Magn. Magn. Mater. **564**, 170211 (2022).
[18] R. Forrer, Ann. Phys.-Paris. **12**, 605 (2017).
[19] V. S. Bai and T. Rajasekharan, J. Magn. Magn. Mater. **42**, 198 (1984).